Published in Q. J. R. Meteorol. Soc. 142: 3152–3161, October 2016 B DOI:10.1002/qj.2896
Preprint version

Evaluation of a wind farm parameterisation in a regional climate model using large eddy simulations

F. Chatterjee[1]* , D. Allaerts[2], U. Blahak[3], J. Meyers[2], N.P.M. van Lipzig[1]

[1]*Department of Earth and Environmental Sciences, University of Leuven, Belgium*

[2]*Department of Mechanical Engineering, University of Leuven, Belgium*

[3]*German Weather Service, Research and Development Department, Offenbach, Germany*

*Correspondence to: Department of Earth and Environmental Sciences, University of Leuven, Belgium.

E-mail:fabien.chatterjee@ees.kuleuven.be

The increasing number of wind farms in the North Sea planned for 2020 is likely to affect the local, regional, and perhaps global climate. To this effect, it is crucial to be able to adequately model wind farms on the regional scale. Wind farms have previously been implemented in regional climate models. However such models have rarely been thoroughly evaluated, due to a lack of observation.

In this study, an idealised version of the COSMO-CLM regional climate model is used in order to evaluate a constant thrust version of the Fitch wind farm parameterisation using large eddy simulations. As a benchmark for the COSMO-CLM and LES comparison, a channel flow without wind farms is first evaluated. COSMO-CLM is able to reproduce this channel flow with an RMSE of 0.6 ms^{-1} (4%) and an Ekman flow with an RMSE of 0.05 ms^{-1} (2%). Next, the wind farm parameterisation is implemented and evaluated. The wind farm parameterisation yields a root mean squared error (RMSE) of 4 ms^{-1} (12%) in wind speed for the channel flow, and an RMSE of 0.2 ms^{-1} (3%) for the Ekman flow. Based on LES output a parameter was introduced to correct for the use of the grid box averaged velocity to calculate the thrust force in the wind farm parameterisation instead of the disk averaged wind speed. This correction had little impact on the RMSE, showing that the use of the grid box velocity in the wind farm parameterisation is adequate.

Key Words: Wind farm parameterisation, Ideal simulation, COSMO-CLM, LES, Constant thrust wind farm parameterisation, Channel flow, Ekman flow

Received . . .

1. Introduction

Offshore wind deployment is foreseen to expand dramatically and solid progress has been made towards 40 GW of offshore wind energy over Europe by 2020 (http://www.ewea.org/policy issues/offshore/ (2015)). This expansion is strongly driven by EU and national policies that aim to provide a higher penetration of renewable energy sources. However, the increasing number of wind farms will reduce open space between them (http://www.4coffshore.com/offshorewind/ (2015)) and will create shadowing effects between wind farms which could affect power production (Adams and Keith (2013), Miller *et al.* (2015)) and could affect local (Zhou *et al.* (2012)), regional (Vautard *et al.* (2014)) and possibly global climate (Wang and Prinn (2010)). Quantifying such potential effects is therefore essential. As a result, an accurate representation of wind farms in climate models is crucial.

In a regional (RCM) and global climate model, multiple wind turbines are present in one grid cell, and inter-turbine flows are not resolved and need to be parameterised. Wind farm parameterisations have already been applied in these models. These parameterisations can be classified in two categories (Fitch *et al.* (2013)). In the first category, the effects of wind farms on the wind flow are represented as elements of increased roughness length. These parameterisations have been used to estimate climatic responses to giant wind farm structures. It was found that these wind farms could cause a synoptic response (Barrie and Kirk-Davidoff (2010), Wang and Prinn (2010)), and cause local cooling in oceans and seas (Barrie and Kirk-Davidoff (2010), Wang and Prinn (2010), Keith (2004)).

Wind farm parameterisations based on such roughness lengths approach do not adequately capture the physics of the effect of wind turbines on the flow (Fitch *et al.* (2013)), as increasing the roughness length induces the strongest deceleration close to the surface, and not at hub height (Fitch *et al.* (2013)). Furthermore, by using the enhanced roughness length approach, wind farm induced surface changes of heat and moisture fluxes were found to be too strong.

In the second category, wind farms are more realistically represented as elevated sinks of momentum and sources of turbulent kinetic energy (TKE) (Blahak *et al.* (2010), Fitch *et al.* (2012), Fitch *et al.* (2013), Fitch (2015)). Changes in surface fluxes are due to the turbines mixing the air column within the wind farm (Roy *et al.* (2004), Roy and Traiteur (2010), Fitch *et al.* (2013)) and this can extend many kilometers downstream of the farm (Roy and Traiteur (2010)). Such parameterisations have been used to quantify the effect of wind farms on the regional (Vautard *et al.* (2014)), and global scale (Fitch (2015)).

In recent years, wind farm parameterisations have been compared to temperature and wind speed measurements. In a regional climate model, Roy *et al.* (2004) and Roy (2011) found that wind farms affected near surface temperatures. Their results agree qualitatively with field measurements (Roy and Traiteur (2010)). Nevertheless, these measurements were taken over a wind farm with different atmospheric conditions than their simulations, thus hampering a quantitative assessment.

In a later study, Fitch *et al.* (2012) simulated an offshore wind park and observed a 10% deficit in the 10 m wind, a fair agreement with the wakes observed behind Horns Rev and Nysted offshore wind farms (Christiansen and Hasager (2005)). Furthermore, a quantitative validation was performed by Jiménez *et al.* (2015). They compared their wind farm parameterisation in an RCM at a 330 m resolution and found good correspondence with an observational data set created from a supervisory control and data acquisition system (SCADA) of the turbines at Horns Rev. They were however unable to resolve inter turbine wake flows, even at such a high resolution. Recently, Volker *et al.* (2015) have compared their simulated wind speeds using a wind farm parameterisation with met mast measurements in the wake of an offshore wind farm. Their results fell within one standard deviation of the wind speeds measured at two meteorological masts.

Due to the difficulty of obtaining wind farm observations, direct evaluation of wind farm parameterisations in RCMs as mentioned above is still limited. On the other hand, large eddy simulations (LES) have been thoroughly evaluated using wind tunnel experiments (Porté-Agel *et al.* (2011), Wu and Porté-Agel (2012), Porté-Agel *et al.* (2014)) and light-detection and ranging (LIDAR) systems (Aitken *et al.* (2014), Mirocha *et al.* (2014)).

These LESs have been used to study the interactions between the atmospheric boundary layer (ABL) and wind turbine arrays.

Furthermore, LES have already been used to develop coarser resolution model parameterisation. For example, Abkar and Porté-Agel (2015), with the aid of an LES have developed a wind farm parameterisation suitable for RCMs. In their study however, the coarse scale wind farm parameterisation was developed with the LES and the assumptions of the parameterisation were evaluated within the LES. There was no evaluation of the parameterisation in an RCM, and it could therefore not be assessed how this coarse scale parameterisation would perform in a regional climate model.

Regional climate models have been evaluated with LES in the past. Fitch *et al.* (2012) have compared their results with LES studies from literature (Lu and Porte-Agel (2011) and Calaf *et al.* (2010)), but differences in boundary conditions and domain height between models resulted in a qualitative evaluation.

This paper is the first to implement a wind farm parameterisation in an RCM and evaluate it against an LES in idealised flow conditions making a direct rigorous quantitative comparison possible. A framework for comparing an RCM against LES data was developed and applied. The aim of this paper is to use this framework in order to evaluate a wind farm parameterisation in an RCM at a resolution suitable for climate simulations. A constant thrust version of the widely deployed Fitch parameterisation (Fitch *et al.* (2012)) was used since the LES had a constant thrust coefficient. Moreover, the robustness of the parameterisation to the configuration of the wind farm is tested. This is done for an infinite wind farm case in neutral conditions, implying that aspects such as wind farm downstream wake effects, or effects of wind farms on atmospheric stability are not evaluated here.

This paper is structured as follows: the theory and set up of the frame work are described in section 2. In section 3.1 the results of flows without wind farms are presented. In section 3.2 comparisons between wind farm LES and wind farm COSMO-CLM simulations are presented. In section 3.3 sensitivity studies are discussed. Finally, in section 4, conclusions are drawn.

2. Theory and Experimental Set Up

In the following subsections, the framework for evaluating a wind farm parameterisation in an RCM against LES is described. Turbulent motions related to total stresses (see section 2.1.1) are resolved in the LES, but are parameterised as sub-grid scale processes in an RCM. Consequently, the LES is used to evaluate the parameterisation in the RCM.

As a first step, the RCM is evaluated against the LES in the absence of wind turbines. This is necessary in order to quantify uncertainties due to the parameterised turbulent motions in the RCM. Subsequently, the effects of wind turbines in the RCM are evaluated against output from an LES wind farm simulation. The sections hereafter further detail this methodology.

2.1. *Idealised model simulation without wind farms*

2.1.1. *Large Eddy Simulations*

In large-eddy simulations (LES), the largest, energy-containing scales are represented explicitly, whereas the smaller, dissipative scales are parameterised. To this extent, the filtered Navier-Stokes equations are solved, and the influence of the unresolved scales is accounted for through a sub-grid scale model. In the current study, an updated version of an LES, SP-Wind (see, e.g. Calaf *et al.* (2010), Goit and Meyers (2015), Meyers and Meneveau (2013), Allaerts and Meyers (2015)) is used. This pseudo-spectral code applies spectral discretization and periodic boundary conditions in the horizontal directions ensuring an infinite flow, and a fourth-order energy-conservative finite difference scheme (Verstappen and Veldman (2003)) in the vertical direction. Temporal advancement is performed with a classic four-stage fourth-order Runge-Kutta scheme.

At the top of the domain, the horizontal stress and the vertical velocity are set to zero (Meyers and Meneveau (2010), Meyers and Meneveau (2013), Calaf *et al.* (2010)). At the lower boundary, classical Monin-Obukhov similarity theory is used to impose a wall stress model (Moeng (1984)). The sub-grid scale stresses are modelled with a standard Smagorinsky model (Smagorinsky (1963)), which is damped near the surface using the classical wall damping function of Mason and Thomson (Mason and Thomson (1992)).

Two sets of LES cases are used for comparison with the RCM, both of which consider a dry, neutral, atmospheric boundary layer. Although the reality is more complex (see for example, Muñoz

Esparza *et al.* (2012)), such an idealised set up is an important first step in evaluating the wind farm parameterisation. In addition, the presented methodology can later be extended to cover different stabilities and moisture content.

In the first set of LES simulations, the influence of the Earth's rotation is neglected so that the atmospheric boundary layer is merely pressure driven. This corresponds to the simulation set up by Calaf *et al.* (2010). It is the first step in developing the framework for evaluating the RCM against the LES, and will serve as a reference simulation. In these cases, the height of the boundary layer coincides with the top of the domain, which is set at 1000 m, and the grid resolution is approximately $24.5\ \mathrm{m} \times 16.4\ \mathrm{m} \times 7.8\ \mathrm{m}$ in x, y and z-direction, respectively. These grid cell dimensions lie within the range of grid resolutions typically used in LES of large wind farms in neutral ABLs (see, e.g., Calaf *et al.* (2010), Calaf *et al.* (2011), Stevens *et al.* (2014), Wu and Porté-Agel (2015)). The rotors will be located in the y-z plane (section 2.1.2), and so these directions have higher resolutions in order to resolve the turbines adequately.

In the second set, the introduction of Coriolis forces in the Navier-Stokes equation leads to a rotating atmospheric boundary layer. The height of the numerical domain is chosen to be 5000 m in order to allow the Ekman layer to freely attain its equilibrium height. Grid resolution in these cases is the same as in the first set.

The horizontal resolution of the LES is much finer than that of an RCM as this generally has a resolution of the order of kilometers in x and y (see figure 1). In order to compare the LES results with the RCM, the wind velocity in each grid box in the LES is first time averaged. This is defined as $\overline{u_i}$, where u_i corresponds to the grid box velocity in the x,y, and z direction corresponding to $i = 1, 2, 3$. The overbar denotes time averaging. Next, for each model layer, the horizontal average over the whole domain is taken (256×192 grid boxes). Therefore, a time and horizontally averaged gridbox velocity, $\langle \overline{u_i} \rangle$, where the brackets denote horizontal averaging, is compared to RCM output.

Furthermore, a fluctuation around the time average velocity component is calculated as $u_i' = u_i - \overline{u_i}$. The Reynold stresses are calculated as $\langle \overline{u_j' u_3'} \rangle$, where $j = 1, 2$, corresponding to the x and y directions. In addition "dispersive stresses" (see Calaf *et al.* (2010) for details) arise due to correlations among the spatially nonhomogeneous mean velocities. These are computed as $\langle \overline{u_j'' u_3''} \rangle$, where fluctuations are defined as $u_i'' = u_i - \langle \overline{u_i} \rangle$. Consequently, the total stresses,τ_{j3}, are calculated as $\langle \overline{u_j' u_3'} \rangle + \langle \overline{u_j'' u_3''} \rangle$. Similarly, the TKE components are calculated as $0.5 \left(\langle \overline{u_i' u_i'} \rangle + \langle \overline{u_i'' u_i''} \rangle \right)$.

In COSMO-CLM, such dispersive stresses are not present due to the coarseness of the grid, and the total stress is equal to the modelled Reynolds stress.

2.1.2. *Regional Climate Model*

In order to create a framework where a wind farm parameterisation can be compared to a wind farm LES simulation, the COSMO model in climate mode (COSMO-CLM, Rockel *et al.* (2008)) in an idealised set up is used (see Schlemmer *et al.* (2011), and Schlemmer *et al.* (2012)). COSMO-CLM solves the compressible non hydrostatic Navier Stokes equations. A 2.5 Mellor-Yamada turbulence scheme (Mellor and Yamada (1982)) is used to parameterise sub-grid scale processes and the mixing length, the Blackadar length scale (Blackadar (1962)), is used.

The two LES cases are modelled in COSMO-CLM with a single column at a 2.8 kilometer resolution. Similar to the LES, in order to simulate an infinite flow, periodic boundary conditions are set in the horizontal directions.

The height coordinates follow the Gal-Chen coordinate system. The top of the model domain is located at 1000 m for the no Coriolis case (or reference flow), and 5000 m for the Coriolis case (or Ekman flow). As in the LES, the higher domain in the latter is necessary to allow for the growth of the Ekman layer. At the top of the domain, zero stress and zero vertical velocity boundary conditions are imposed. These cases have 10 and 30 layers respectively, corresponding to the vertical resolution typically used for climate simulations (for example Van Weverberg *et al.* (2014), Brisson *et al.* (2015)). Such resolutions were chosen in order to evaluate the wind farm parameterisation at a vertical resolution typical for climate simulation.

Neutral conditions are enforced by applying a constant temperature lapse rate of $-g/c_p$, where g is the acceleration due to gravity and c_p is the gas constant at constant pressure and no moisture is present in the model.

At the surface, the boundary conditions are modelled by a standard bulk transfer scheme. A pressure gradient force is prescribed in order to force the flow. The wind profile can evolve freely until steady state is reached. This occurs when the pressure gradient force is balanced by friction at the surface, $dp/dx = d\tau/dz$ (Pope (2000)), where p is pressure, and τ is the total stress.

The total frictional forces are a direct consequence of the prescribed pressure gradient, and the wind speed evolves under these constraints. The pressure gradient induces a linear decrease of the shear stress from its value at the surface, to the top of the domain (Pope (2000)). When the model reaches a steady state, the wind speed follows the classical logarithmic wind profile (see for example Stull, R. B. (1988)):

$$U = \frac{u_*}{\kappa} \ln \frac{z}{z_0} \tag{1}$$

where u_* is the friction velocity at the surface. The roughness length, z_0, is set to 10^{-4} m and $\kappa = 0.4$ is the von Kármán constant. COSMO-CLM is forced by a pressure gradient force of 1.6×10^{-4} ms^{-2}. This gives a velocity of 16.1 ms^{-1} at 1000 m height in the absence of a windfarm.

In order to save computational time, the model is initialised with the same wind velocity profile as equation 1. Since the final wind profile is the result of the balance between drag forces and the pressure gradient force, the initial profile has little influence on the final wind velocity. Furthermore the flow is homogeneous in the horizontal directions and variations are only present in the vertical. The model reaches a steady state after 116 hours and its output is compared to data from the LES. Steady state is defined when wind speed variations with time at all heights are 10^{-4} ms^{-1} or smaller.

This set up is first tested by comparing COSMO-CLM in the absence of wind farms. This COSMO-CLM simulation without Coriolis, hereafter named the CCLM-NWF case (see table I for a summary of the experiments), is compared with its no Coriolis LES counterpart: the LES-NWF case.

The same comparison is then made between COSMO-CLM and the LES, but this time with Coriolis effect included, referred to as the CCLM-NWF_C and the LES-NWF_C cases, respectively. In these cases, the pressure gradient force is set to 10^{-3} ms^{-2} in the meridional direction, and the Coriolis parameter to 10^{-4} s^{-1}, resulting in an upwards pointing rotation vector. The geostrophic wind is therefore 10 ms^{-1} in the zonal direction.

In the Coriolis case, the flow evolves freely until a balance between the Coriolis force, surface friction and the pressure gradient force is reached. Close to the surface, due to friction an ageostrophic component is present resulting in an Ekman spiral. The balance therefore is more complex than the simple no Coriolis case, and this can have implications on the shear stresses and TKE as will be shown in section 3. The boundary conditions are identical as the no Coriolis cases.

As described in the next section, the LES is used in order to evaluate the wind farm parameterisation. The evaluation performed in this article represents an evaluation under idealised conditions. The atmsophere is neutrally stratified and does not contain moisture. Moreover, the wind farm parameterisation is evaluated for an infinite wind farm situation and therefore wake effects are not evaluated here.

2.2. *Idealised model simulations with wind farms*

In this section, the implementation of the wind turbines in COSMO-CLM and the LES are outlined. Further details on the implementation in the LES can be found in Calaf *et al.* (2010) and Meyers and Meneveau (2010), while details of the implementation of the wind turbines in COSMO-CLM can be found in Fitch *et al.* (2012).

Wind turbines extract kinetic energy from atmosphere therefore decelerating the flow and will modify the momentum equation as follows

$$\frac{\partial u_i}{\partial t} = \ldots - FD_i \tag{2}$$

where u_i represents the grid velocity in the x ($i = 1$) or y ($i = 2$) direction in either the LES or COSMO-CLM. It is assumed that the wind turbine thrust force on the vertical velocity is negligible. The ellipsis represents the other terms in the Navier-Stokes equation, such as the pressure gradient and Coriolis force, and viscous dissipation, (see for example Stull, R. B. (1988) for further details). FD_i is the thrust force per unit mass due to the

Table I. List of Simulations

accronym	Coriolis	C_T	Staggering
COSMO-CLM			
CCLM-NWF	no	NA	none
CCLM-WF	no	$3/4$	none
CCLM-WF+	no	$1.11 \times 3/4$	none
CCLM_C	yes	NA	none
CCLM-WF_C	yes	$3/4$	none
CCLM-WF_C+	yes	$1.11 \times 3/4$	none
LES			
LES-NWF	no	NA	none
LES-WF	no	$3/4$	none
LES-NWF_C	yes	NA	none
LES-WF_C	yes	$3/4$	none
LES-WFS	no	$3/4$	Single
LES-WFS_C	yes	$3/4$	Single
LES-WFDS	no	$3/4$	Double
LES-WFDS_C	yes	$3/4$	Double

wind turbine, whose implementation in the LES and COSMO-CLM is outlined here. Without wind farms, this term is equal to zero.

2.2.1. *Large Eddy Simulation*

The representation of wind turbines in this LES is based on a classical expression for a stand-alone wind turbine (see, for example Burton *et al.* (2001) and figure 1a), where the flow is approximated as being one dimensional. The thrust force due to a single turbine is given by:

$$F = -\rho \frac{1}{2} C_T u_\infty^2 \frac{\pi}{4} D^2, \tag{3}$$

where, D is the diameter of the rotor, u_∞ is the undisturbed upstream velocity, ρ is the total air density, and C_T is the thrust coefficient. According to the Betz theory, C_T is a function of u_∞ and u_d, the velocity at the disk. From this expression, FD_i is derived for the LES.

In a wind farm, wakes from turbines interact with other turbines (figure 1b)) making it difficult to define a suitable value for u_∞. In the LES, a different method for calculating the thrust force is implemented. The turbines are modelled with a so called actuator disk model (ADM) (Jimenez *et al.* (2007), Jimenez *et al.* (2008), Meyers and Meneveau (2010), Calaf *et al.* (2010), Meyers and Meneveau (2013)). This method has been proven to adequately represent wakes at a distance larger than 3 times the diameter of the rotor (D) in the x direction (Wu and Porté-Agel (2012)), and yields a good representation of the interaction of the wind farms with the boundary layer (Goit and Meyers (2015)). In this method, every turbine is represented by a porous disk that exerts a thrust force on the flow which is computed as

$$F_{tLES} = -\rho \frac{1}{2} C_T' \langle \bar{u}^T \rangle_d^2 \frac{\pi}{4} D^2, \tag{4}$$

where F_{tLES} represents the thrust force as calculated in the LES. Instead of u_∞ (equation 3), which within a wind farm is difficult to estimate, the local disk-averaged time-filtered velocity, $\langle \bar{u}^T \rangle_d^2$ is used, together with disk-based thrust coefficient C_T'.

The thrust force is first distributed constant over the disk area on a fine grid in the turbine rotor plane. FD_i is then obtained by filtering the force per unit mass in the turbine rotor plane onto the coarser LES grid by means of a Gaussian convolution filter (Calaf *et al.* (2010)).

The wind farm parameterisation in the LES simulates idealised wind turbines where C_T' is derived using blade element theory (eg appendix A of Goit and Meyers (2015), Meyers and Meneveau (2010, 2013)) and is the result of the integrated drag and lift coefficients, blade geometry and flow angles. In such turbines, it is assumed that below the rated wind speed the turbines use a generator-torque control to keep the tip speed ratio at its optimal value. Furthermore the blade pitch is kept constant at its optimal design value (Goit and Meyers (2015)). In an ADM this implies a constant disk based thrust coefficient (Goit and Meyers (2015), Meyers and Meneveau (2010, 2013)).

This coefficient is estimated using the following relation (see Calaf *et al.* (2010), Meyers and Meneveau (2010), Abkar and Porté-Agel (2015)):

$$C_T' = C_T/(1-a)^2 \tag{5}$$

where C_T is the classical thrust coefficient and a represents the induction factor. Using results from previous LES studies (eg Calaf *et al.* (2010), Meyers and Meneveau (2010), Goit and Meyers (2015)), $C_T = 0.75$, and $a = 0.25$, resulting in $C_T' = 4/3$. The value of C_T and a were taken from Jimenez *et al.* (2007). This value of C_T is also used in COSMO-CLM, in order to ensure a fair comparison with the LES. This value of C_T is slightly higher than the maximum thrust coefficient used by Vautard *et al.* (2014).

The wind turbines are evenly distributed on the grid with a spacing of approximately 700m and 500m in the x and y directions. Furthermore, the turbines are aligned with the flow. In the present paper, the full domain is covered by wind turbines. With periodic boundary conditions, the wind farm is essentially infinite.

2.2.2. *Regional Climate Models*

In RCMs, a much coarser resolution is used than in the LES (see section 2.1), and multiple turbines are contained within one grid box (as depicted by the hatched box in figure 1c). The individual wind turbines- with their wake effects- are not resolved and so the grid box velocity, U_i in figure 1c, is used to emulate an average effect of these turbines. The thrust force is therefore parameterised with the grid box velocity as the profiles of u_∞ and $\langle \bar{u}^T \rangle_d$ are not resolved.

For each layer intersecting the rotor area, the wind turbines extract mean kinetic energy from the flow. As a result, for each layer in the grid box, the wind will experience a deceleration:

$$\frac{\partial |U|}{\partial t} = -\frac{1}{2}\frac{N C_T |U|^2 A}{\Delta z} \tag{6}$$

where N represents the number of wind farms per m^2, C_T represents the thrust coefficient, described above, and A represents the area of the rotor intersecting the layer thickness Δz. In the present case there are 6 $\times$ 8 wind turbines in an LES domain of about 18 km^2, corresponding to a wind turbine density of approximately 2 $\times$ 10^{-6} m^{-2}. In component form equation 6 results in

$$FD_i = \frac{U_i}{|U|}\frac{\partial |U|}{\partial t} \tag{7}$$

see Fitch *et al.* (2012) for the full derivation. For each layer intersecting the rotor area, the deceleration is dependent on the thrust coefficient, wind speed, and density of the wind turbines.

The remaining part of the energy is converted into turbulent kinetic energy. This process is resolved in the LES, but has to be parameterised in COSMO-CLM as follows. The fraction of energy converted into electricity by the turbine is characterised by C_P. The fraction of energy generating TKE by the turbines is estimated using $C_{TKE} = C_T - C_P$, and the amount of TKE converted by the wind turbines is given by (Fitch *et al.* (2012)):

$$TKE_{wf} = \frac{1}{2}\frac{N C_{TKE} |U|^3 A}{\Delta z} \tag{8}$$

The present LES simulations do not calculate the disk based power coefficient C_P' and therefore C_P in equation 8 cannot be derived from LES. It was therefore calculated using linear Betz theory, where $C_P = (1-a)C_T$.

This extra TKE term increases the mixing of the turbine through turbulent motion. It does not reproduce individual wakes from different turbines (Fitch (2015)).

The TKE_{wf} term modifies the TKE equation in COSMO-CLM in the following way:

$$\frac{\partial q^2}{\partial t} = \ldots + TKE_{wf} \tag{9}$$

where q is the turbulent velocity scale and $q^2 = 2 \times TKE$. The ellipsis in the equation represent other terms in the TKE equation such as TKE creation by mechanical shear, buoyancy flux, dissipation of TKE and turbulent transport (see Doms *et al.* (2005) for details).

Two simulations are performed in the LES and COSMO-CLM in the presence of wind farms, referred to as the LES-WF and CCLM-WF cases for the no Coriolis cases. For the Coriolis cases the presence of wind farms simulations are denoted as CCLM-WF_C and LES-WF_C respectively. In order to make the comparisons fair, in both the LES and COSMO-CLM, following

Calaf *et al.* (2010), Meyers and Meneveau (2010), Goit and Meyers (2015), the rotor has a radius of 50 m, with the hub height located at 100 m. Additionally, the wind turbine density N, in COSMO-CLM also matches the number of turbines per m^2 in the LES.

Furthermore, two additional cases were simulated with the LES: a staggered wind farm, hereafter the LES-WFS case, and a doubly staggered one, named the LES-WFDS case. In such cases, the turbine rows are no longer aligned as rows are shifted with respect to one another, and a turbine may not necessarily be in the wake of the one in front of it. Staggering a wind farm is analogous to changing the inflow angle. In the present cases the staggered and doubly staggered represent inflow angles of 12.53° and 18.43° respectively. Different inflow direction will lead to different turbine wake interactions in the LES as a wake from a turbine might not reach the next turbine. This in turn will lead to different momentum dissipation.

In the present case of the infinite wind farm, COSMO-CLM is unable to capture such differences in turbine wake interaction within a wind farm since the grid is too coarse to resolve individual turbines. Consequently, these two cases provide an estimate of the range of uncertainty related to the inflow direction. The staggered and the doubly staggered cases are also considered for the LES simulations with Coriolis. These are denoted as the LES-WFS_C and the LES-WFDS_C cases respectively.

2.3. *Sensitivity of the wind farm momentum sink*

As stated earlier, due to COSMO-CLM's coarse horizontal resolution, the grid box velocity is used, to calculate the average drag of the turbines on the grid cell. This is not the case in the LES, where the drag is calculated using the disk averaged wind speed. By diagnosing the LES' output, it is possible to quantify the effect of using the grid box average velocity instead of the disk based velocity.

This is done in the LES the following way. A thrust force, F_{tDAV} using the horizontally domain averaged velocity U(z), as opposed to the disk averaged velocity, is defined. In order to calculate the overall effect of the rotor, this velocity is integrated over the wind farm rotor area:

$$F_{tDAV} = \frac{1}{2}\rho C_T \int_A U(z)^2 \, dA' \tag{10}$$

Similarly to equation 3, C_T is used instead of C_T'. The bias of using the horizontally averaged velocity is estimated by comparing F_{tDAV} with equation 4:

$$\xi = \frac{F_{tLES}}{F_{tDAV}} \tag{11}$$

where ξ is the relative bias. To correct for this bias in COSMO-CLM, equation 7 is multiplied by ξ:

$$FD{+}_i = \xi \frac{U}{|U|} \frac{\partial |U|}{\partial t} \tag{12}$$

where $FD{+}_i$ represents the modified momentum thrust force of the turbine. The CCLM-WF and CCLM-WF_C cases are then repeated using $FD{+}_i$ instead of FD_i and are called the CCLM-WF+ and CCLM-WF_C+ cases respectively.

Note that such an analysis is similar to that of Abkar and Porté-Agel (2015), who calculates the ratio of the undisturbed wind speed to the grid averaged wind velocity. The results are described in section 3.3.

3. Results

3.1. *Idealised model simulations without wind farms*

The wind speed profiles in the absence of wind farms are shown in figure 2a. There is a good agreement between the output from CCLM-NWF and the LES-NWF curves, with a root mean square error (RMSE) of 0.6 ms^{-1} or 4%. The CCLM-NWF case has a 11% steeper gradient (du/dz) than the LES-NWF case. This difference in gradient between the wind speeds profiles are due to the differences in TKE profiles shown in figure 2b. The weaker TKE in COSMO-CLM results in less mixing and a stronger wind gradient. The RMSE for TKE is about 0.1 m^2s^{-2} or 22%. The total stresses for the reference flow (not shown) decrease linearly from their surface value to zero at the top of the domain in both the LES and COSMO-CLM (see eg. Calaf *et al.* (2010) and section 2.1).

In a subsequent step, COSMO-CLM was compared with output from an LES for an Ekman flow (the Coriolis case). The RMSE for the wind speed is approximately 0.05 ms^{-1} (2%) (figure 2 c). The

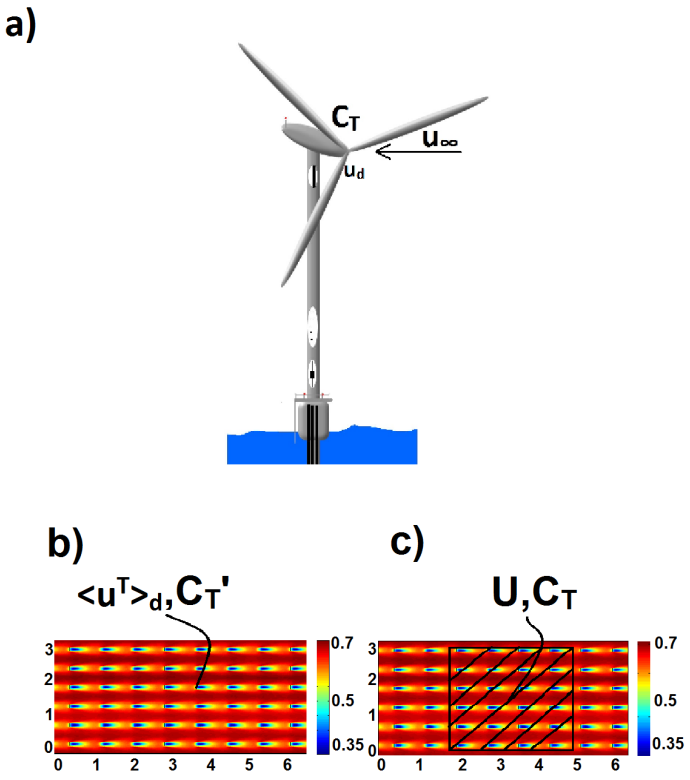

Figure 1. a) A single turbine b) Top view LES wind speed normalized by the geostrophic wind for a domain of 6 x 3 km. The thrust coefficient (C_T') and the wind velocity at the disk ($\langle \bar{u}^T \rangle_d$) defined at the disk and are used to calculate the LES disk based thrust. c) Same as b) with a schematic of the COSMO-CLM grid box over the LES domain. The grid box in COSMO-CLM is coarser and the grid box velocity U, with the thrust coefficient C_T are used to calculate the averaged wind turbine thrusts on the grid.

wind angles are in good agreement. A jet structure is visible and is due to the fact that the total stresses have a component in the direction of the Coriolis force (Johnstone and Coleman (2012)), generating a super-geostrophic jet. There are discrepancies in the TKE, with an RMSE of 0.02 m^2s^{-2} (18%), which results in an RMSE of 0.002 m^2s^{-2} (5%) for the total stresses (figures 2 e and f). Although the TKE in the CCLM-NOWF_C, is less than its LES counterpart, due to COSMO-CLM's steeper gradient in wind speed, the total stresses are slightly larger in COSMO-CLM than in the LES.

With small RMSEs in wind speed for no Coriolis and Coriolis cases respectively, COSMO-CLM is able to reproduce an LES flow with no significant deterioration, related to the difference in TKE representation. Therefore, the present framework can be used to evaluate the wind farm parameterisation with LES keeping in mind that the TKE in COSMO-CLM can have substantial deviations.

3.2. *Idealised model simulation with wind farm*

In this section, the wind farm parameterisation is evaluated against LES data for both a reference and an Ekman flow. For the reference flow, the wind speed has an RMSE of 0.6 ms^{-1} (or 12%) which is larger than the uncertainty due to model set up (figure 3a). Two logarithmic layers are seen, one that is going from the surface to the lower edge of the wind turbine and one going from the upper edge of the wind turbine to the top of the domain. The wind turbines act as a second rough surface (Frandsen (1992), Calaf *et al.* (2010)). In the LES-WF case, a third layer is seen within the rotor area, as described by Calaf *et al.* (2010). This has also been observed by Porté-Agel *et al.* (2011) using sonic detection and ranging (SODAR) measurements at an 11 km^2 wind farm, under near neutral conditions, located in Mower County, Minesota. The CCLM-WF case is unable to capture this feature, due to the coarse vertical resolution. However, the region above the rotor area shows the expected logarithmic wind speed profile. The vertical gradients of the wind speeds, above the rotor, is 27%

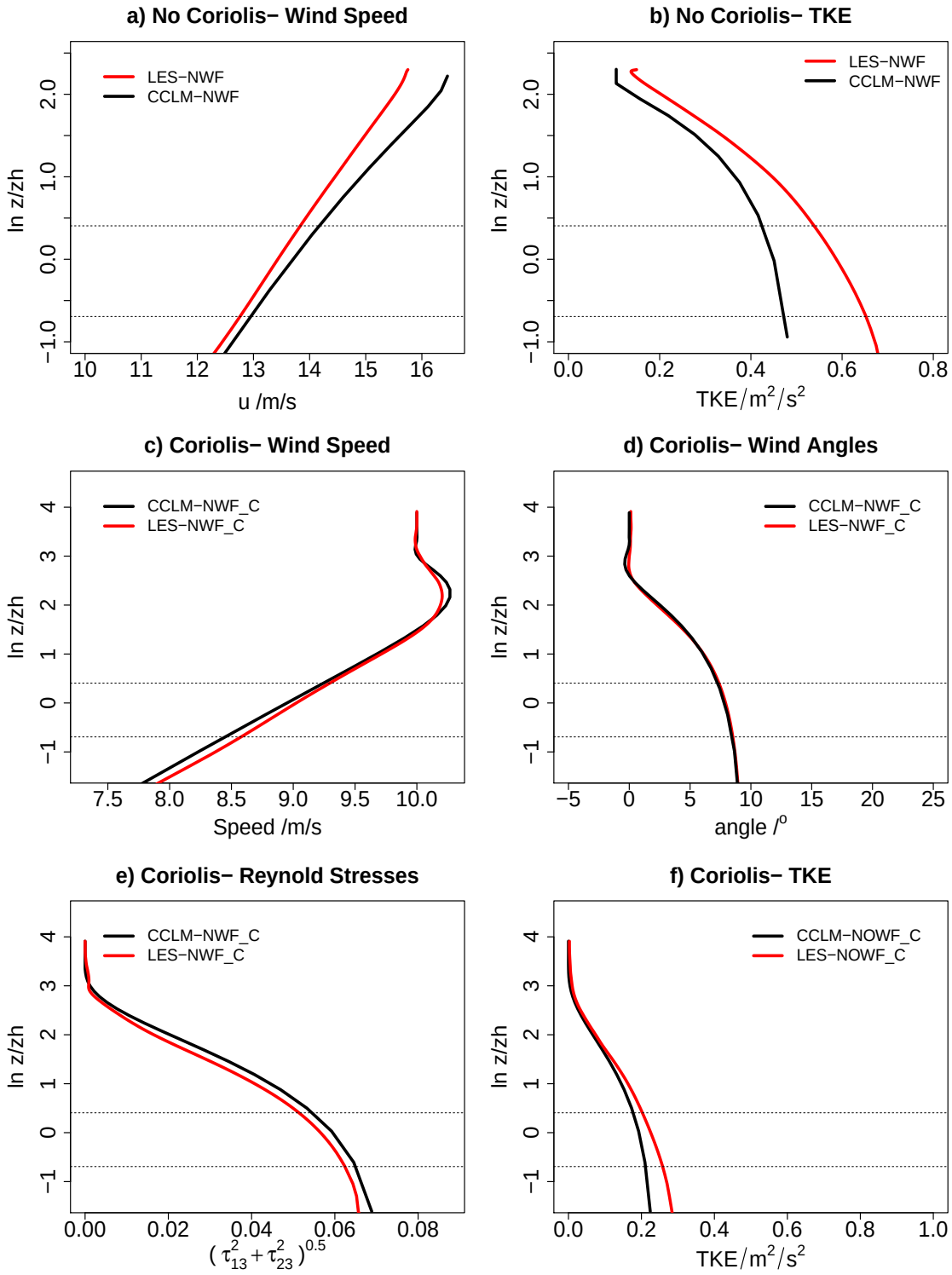

Figure 2. No Wind farm: a) Reference flow: horizontal wind b) Reference flow: TKE, c) Ekman flow: Wind Speed d) Ekman flow: Wind angle with geostrophic flow e) Ekman flow: Total Stresses f) Ekman flow: TKE. The vertical axes show the logarithm of height, normalized by the hub height, z_h.

larger in the CCLM-WF compared to the LES-WF case.

The wind speed profile slightly differs from those shown in Fitch *et al.* (2012) and Roy *et al.* (2004) as no acceleration at the surface is observed. This is due to the different vertical grid set up used here. In any case, we do observe a good correspondence near the surface between CCLM-WF and LES-WF.

The total stresses for the LES-WF and CCLM-WF cases, are highest at the top of the rotor (figure 3b). Within the rotor area, the drag depletes the momentum, until the ground is reached (Calaf *et al.* (2010)). Above the turbine area, the total stresses decrease linearly until the top of the boundary as described in section 2.1.2.

Despite the fact that the shear stresses are maximum at the rotor top, the TKE for both the CCLM-WF and the LES-WF case is largest within the rotor area (figure 3c). This is adequately

modelled in COSMO-CLM by adding an extra TKE term due to wind farms, using equation 8.

The RMSE of the wind speed for the CCLM-WF_C case was found to be about 0.2 ms^{-1} (3%), which is not much larger than the RMSE due to model set up (section 3.1). The nose of the jet is higher for the LES case than COSMO-CLM cases (3d and e).

There is a slight discrepancy in the wind angle, especially in the layers close to the surface (figure 3e), with a bias of 4 degrees at the surface (positive is defined as anti-clockwise). The work done by the flow in COSMO-CLM at the surface, is dependent on the angle of the flow with respect to the pressure gradient force (Johnstone and Coleman (2012)). Furthermore, in the COSMO-CLM case, the nose of the jet is slightly lower than in the LES. The total stresses are somewhat lower in COSMO-CLM (figure3g), which is in contrast with figure 2e, where in the absence of wind turbines, the total stresses are larger in COSMO-CLM than in the LES. The Ekman turning therefore shows a different response to the wind turbines in COSMO-CLM than in the LES.

Similarly to the reference flow case in figure 3c, the TKE for the CCLM-WF_C case is weaker with an RMSE of 0.4 m^2s^{-2} or 66% (figure 3g). As a result, the total stresses above the rotor area are smaller, and the air column is less well mixed. This may be the reason why the Ekman spiraling in figure 3e is stronger in COSMO-CLM (Volker (2014)), and this is perhaps related the TKE scheme used in COSMO-CLM. The TKE increase due to the presence of wind farms in the Coriolis case is well represented in COSMO-CLM (figure 3g and 4a). However the magnitude is too small. Note also that, in contrast to the Coriolis case, in the no Coriolis case, with the additions of wind turbines, the overall TKE decreases and this is well represented in COSMO-CLM (figure 4a and b).

Despite these discrepancies, within the rotor area, the wind speed falls close to or within the uncertainty range provided by the staggered cases (figures 3a and d). Despite of the large RMSEs in TKE, the total stresses compare quite well, and have a mean RMSE of 0.04 m^2s^{-2} or 36% (figure 3f). This falls outside the uncertainty range due to model set up. Despite this, the total mean RMSE for the wind speed over all heights falls within the uncertainty range due to model set up (section 3.1). The wind farm parameterisation, therefore performs well in both Ekman and reference flow.

3.3. *Sensitivities on the thrust force*

As outlined in section 2, a grid averaged wind speed is used in calculating the wind farm thrust coefficient in equation 7, instead of to the rotor averaged wind speed in equation 4.

The correction factor, ξ (see section 2.3) was estimated in the LES was found to be 1.11 for both the reference and Ekman flow (table II). As a result, using a grid box averaged wind speed in COSMO-CLM leads to a weaker drag. The correction factor ξ is implemented in COSMO-CLM as shown in equation 12.

Using this correction factor reduces the RMSE in the no Coriolis case from 0.6 ms^{-1} to 0.4 ms^{-1} (a reduction of 3%) (figure 3a). Originally, COSMO-CLM does not extract enough mean kinetic energy from the flow, compared to the LES (figure 3a). Increasing the forcing by 11% (equation 12) increases the energy extraction therefore reducing the RMSE. For the Coriolis case (figure 3d) the RMSE is hardly affected (RMSE of 0.25 ms^{-1} to 0.26 ms^{-1} for the uncorrected and corrected case respectfully). Therefore, the approximation of using a thrust force based on a grid averaged velocity in a wind farm parameterisation is valid.

The TKE of the flow had the largest RMSE (figures 3c, g and section 3.2). Therefore, an extra sensitivity analysis was performed where the TKE in equation 8 was increased and decreased by a 10% and 20%. However, it was found that increasing or decreasing the term in equation 8 had little effect on the wind speed, angle and total stresses in figure 3 (not shown). As such the TKE term in the wind farm parameterisation plays a secondary role when compared to the momentum sink term (Fitch *et al.* (2012)).

Finally, the assumption was made that the Betz theory holds in a wind farm. Therefore this assumption was used to calculate C_T (equation 5) and C_P in section 2.2. This approximation is verified in the LES by taking the centerline velocity through a wind turbine, and defining an undisturbed wind speed, $u_{wf\infty}$ as the highest velocity in front of the rotor, and a wake velocity, u_{wake}, as the lowest velocity behind the rotor. The latter will be compared to the wake velocity calculated using Betz theory, $u_{wakeB} = u_{wf\infty}(1-2a)$, where $a = C_T'/(4+C_T')$. It was found that the

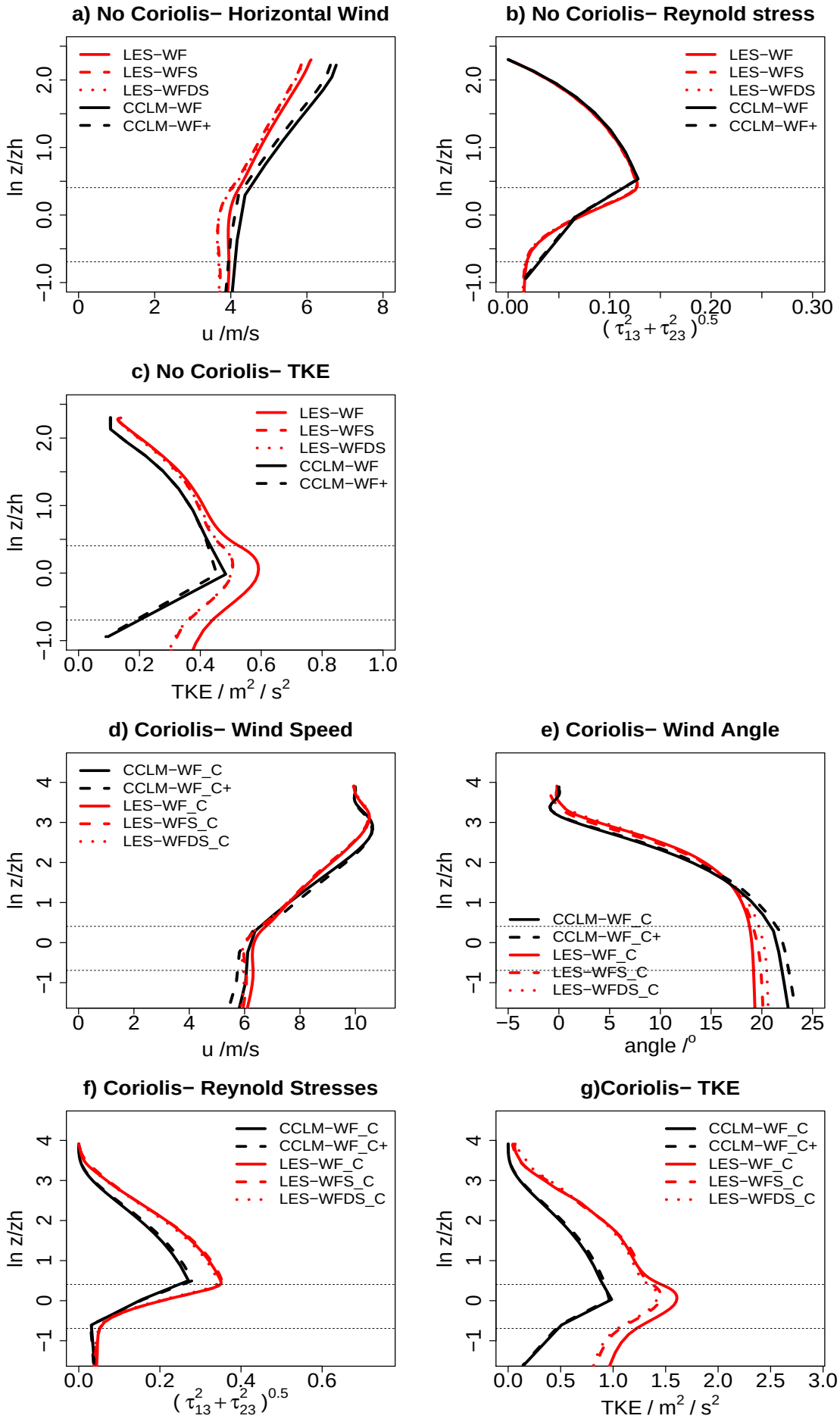

Figure 3. Wind farm: a) Reference flow: horizontal wind b) Reference flow: Total Stresses c) Reference flow: TKE, d) Ekman flow: Wind Speed e) Ekman flow: Wind angle with geostrophic flow f) Ekman flow: Total Stresses g) Ekman flow: TKE. The dashed lines show the sensitivity experiments. The vertical axes show the logarithm of height, normalized by the hub height, z_h.

Table II. Numerical values related to ξ

	Reference flow			Ekman flow		
	Align.	Stagg	D. Stag	Align.	Stagg	D. Stag
ξ	1.11	1.26	1.26	1.11	1.27	1.25

difference between the directly modelled and estimated wake velocity for the Coriolis and no Coriolis case is 0.1 ms^{-1} and 0.07 ms^{-1} respectively. Using Betz theory in calculating the thrusts and power coefficients within a wind farm is therefore a valid approximation.

4. Conclusions

This paper evaluates a constant thrust version of the Fitch wind farm parameterisation, using output from large eddy simulations (LES) for a dry, neutrally stratified idealised pressure-driven boundary layer flow with and without Coriolis force. First, the representation of this idealised flow in COSMO-CLM was tested without wind farms. It was found that wind speeds compare well with those from LES simulations with RMSEs of 0.6 ms^{-1} and 0.05 ms^{-1} for the no Coriolis and Coriolis cases respectively.

The effect of wind farms was found to be correctly represented by the wind farm parameterisation with RMSEs similar or slightly larger than the cases without wind farms. A slight overestimation of wind speeds of 0.6 ms^{-1} was introduced in the case without Coriolis force. For the Coriolis case, the drag in COSMO-CLM was overestimated, resulting in a slight underestimation of the height of the nose of the supergeostrophic jet and an overestimation of the turning of the wind by 4° near the surface.

Based on theoretical considerations and analysing LES output, a parameter ξ was introduced in the wind farm parameterisation. This parameter accounts for the fact that in the derivation of the momentum sink in the wind farm parameterisation, the disk averaged velocity is approximated by the grid box average wind speed. It was found that this refining slightly reduces the RMSE in the no Coriolis case by 0.2 ms^{-1}. The total stresses and TKE are hardly affected by the introduction of the ξ parameter. Overall, there is little difference between the wind farm parameterisation, and the wind farm model in the LES. The approximation of using different thrust forces in the LES compared to COSMO-CLM is of limited impact.

In summary, it is concluded that the wind farm parameterisation can to a large extent adequately represent the effects of wind farms on the profile in COSMO-CLM. There are certain features that are not captured such as the change in wind speed gradient within the rotor area, due to the coarse vertical resolution.

Finally, the wind farm parameterisation has been compared to an LES under the same conditions as the LES. Due to the high resolution of LES, and therefore better representation of COSMO-CLM's subgrid scale processes, the LES provides a valid tool for evaluating a parameterisation designed for regional scale modelling. However, this set up was idealized in both the LES and COSMO-CLM. Impacts on atmospheric stability and humidity, for example were not evaluated. Furthermore, it would be interesting to see how the wind farm parameterisation would behave under a different TKE scheme for COSMO-CLM. A detailed analysis of the TKE components with and without wind farms, for both the Coriolis and no Coriolis case in COSMO-CLM would therefore add insights into behaviour of the wind farm parameterisation.

Moreover, based on section 3.2 (figures 4a and b), the changes in TKE with and without wind farms are different depending on whether or not Coriolis is present. Investigating the energy balance of the mean and turbulent kinetic energy could aid in an improved understanding of the different TKE behaviour in the wind farm parameterisation in the Coriolis and no Coriolis case. This is the subject of further research.

Moreover, in simulating an infinite wind farm, wind farm wake structures were not evaluated here. The wind turbines represented here were constant thrust ones and it would be interesting to see how the wind speed profile would vary had a varying thrust wind farm been simulated. Further research is necessary to test whether the findings in an idealised set-up would hold for real atmospheric conditions and non-idealized wind turbines.

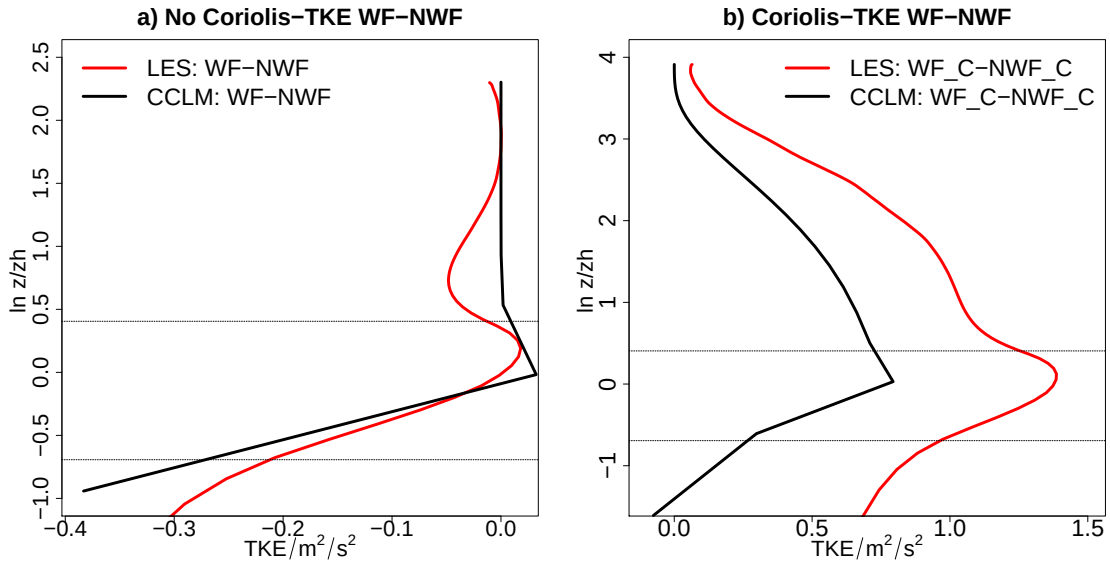

Figure 4. Reference flow: a) No Coriolis: TKE difference between the wind farm and the no wind farm cases for both LES and CCLM. b) same as a) but for the Coriolis case. The vertical axes show the logarithm of height, normalized by the hub height, z_h.

Acknowledgements

The authors acknowledge support from BOF KU Leuven (grant no. IDO/11/012). The authors further acknowledge support from the European Research Council (FP7-Ideas, grant no. 306471), and the Flemish Science Foundation (FWO, grant no. G.0376.12). Simulations were performed on the computing infrastructure of the VSC Flemish Supercomputer Center, funded by the Hercules Foundation and the Flemish Government.

References

Abkar M, Porté-Agel F. 2015. A new wind-farm parameterization for large-scale atmospheric models. *Journal of Renewable and Sustainable Energy* **7**(1): 013 121, doi:10.1063/1.4907600.

Adams AS, Keith DW. 2013. Are global wind power resource estimates overstated? *Environmental Research Letters* **8**(1): 015 021, doi:10.1088/1748-9326/8/1/015021.

Aitken ML, Kosović B, Mirocha JD, Lundquist JK. 2014. Large eddy simulation of wind turbine wake dynamics in the stable boundary layer using the weather research and forecasting model. *Journal of Renewable and Sustainable Energy* **6**(3): 033137, doi:http://dx.doi.org/10.1063/1.4885111.

Allaerts D, Meyers J. 2015. Large eddy simulation of a large wind-turbine array in a conventionally neutral atmospheric boundary layer. *Physics of Fluids* **27**(6): 065 108, doi:10.1063/1.4922339.

Barrie D, Kirk-Davidoff DB. 2010. Physics Weather response to a large wind turbine array. In: *Atmospheric Chemistry and Physics*, vol. 10. pp. 769–775.

Blackadar K. 1962. The Vertical Distribution of Wind and turbulent exchange in a neutral atmosphere. *Journal of Geophysical Research* **67**: 3095–3102.

Blahak U, Goretzki B, Meis J. 2010. A simple parameterization of drag forces induced by large wind farms for numerical weather prediction models. *European Wind Energy Conference and Exhibition 2010, EWEC 2010* **6**(1): 4577–4585.

Brisson E, Demuzere M, Lipzig NPMV. 2015. Modelling strategies for performing convection-permitting climate simulations. *Meteorologische Zeitschrift* doi:10.1127/metz/2015/0598.

Burton T, Jenkins N, Bossyani E. 2001. *Wind Energy Handbook*. Wiley: New York.

Calaf M, Meneveau C, Meyers J. 2010. Large eddy simulation study of fully developed wind-turbine array boundary layers. *Physics of Fluids* **22**(1): 015 110, doi:10.1063/1.3291077.

Calaf M, Parlange MB, Meneveau C. 2011. Large eddy simulation study of scalar transport in fully developed wind-turbine array boundary layers. *Physics of Fluids* **23**(12): 126603, doi:http://dx.doi.org/10.1063/1.3663376.

Christiansen MB, Hasager C. 2005. Wake effects of large offshore wind farms identified from satellite SAR. *Remote Sensing of Environment* **98**(2-3): 251–268, doi:10.1016/j.rse.2005.07.009.

Doms G, Forster J, Heise E, Herzog HJ, Raschendorfer M, Schrodin R, Reinhardt T, Vogel G. 2005. A description of the Nonhydrostatic Regional Model LM. Part 2: Physical parameterizations. Technical report, Deutscher Wetterdienst (DWD), Offenbach.

Fitch AC. 2015. Climate impacts of large-scale wind farms as parameterized in a global climate model. *Journal of Climate* **28**(15): 6160–6180, doi:10.1175/JCLI-D-14-00245.1, URL http://dx.doi.org/10.1175/JCLI-D-14-00245.1.

Fitch AC, Olson JB, Lundquist JK. 2013. Parameterization of Wind Farms in Climate Models. *Journal of Climate* **26**(17): 6439–6458, doi:10.1175/JCLI-D-12-00376.1.

Fitch AC, Olson JB, Lundquist JK, Dudhia J, Gupta AK, Michalakes J, Barstad I. 2012. Local and Mesoscale Impacts of Wind Farms as Parameterized in a Mesoscale NWP Model. *Monthly Weather Review* **140**(9): 3017–3038, doi:10.1175/MWR-D-11-00352.1.

Frandsen S. 1992. On the wind speed reduction in the center of large clusters of wind turbines. *Journal of Wind Engineering and Industrial Aerodynamics* **39**: 251–265.

Goit J, Meyers J. 2015. Optimal control of energy extraction in wind-farm boundary layers. *Journal of Fluid Mechanics* **768**: 5–50, doi:10.1017/jfm.2015.70.

http://www4coffshorecom/offshorewind/. Accessed: 11/06/2015.

http://wwweweaorg/policy issues/offshore/. Accessed: 11/06/2015.

Jimenez a, Crespo a, Migoya E, Garcia J. 2007. Advances in large-eddy simulation of a wind turbine wake. *Journal of Physics: Conference Series* **75**: 012 041, doi:10.1088/1742-6596/75/1/012041.

Jimenez A, Crespo A, Migoya E, Garcia J. 2008. Large-eddy simulation of spectral coherence in a wind turbine wake. *Environ. Res.* **3**(1): 015 004.

Jiménez PA, Navarro J, Palomares AM, Dudhia J. 2015. Mesoscale modeling of offshore wind turbine wakes at the wind farm resolving scale: a composite-based analysis with the weather research and forecasting model over horns rev. *Wind Energy* **18**(3): 559–566, doi:10.1002/we.1708.

Johnstone R, Coleman G. 2012. The turbulent Ekman boundary layer over an infinite wind-turbine array. *Journal of Wind Engineering and Industrial Aerodynamics* **100**(1): 46–57, doi:10.1016/j.jweia.2011.11.002.

Keith D. 2004. The influence of large-scale wind power on global climate. *Proceedings of the ...* **101**(46): 16 115–16 120.

Lu H, Porte-Agel F. 2011. Large-eddy simulation of a very large wind farm in a stable atmospheric boundary layer. *Physics of Fluids* **23**(6): 065 101, doi:10.1063/1.3589857.

Mason PJ, Thomson DJ. 1992. Stochastic backscatter in large-eddy simulations of boundary layers. *J. Fluid Mech.* **242**: 51–78, doi:10.1017/S0022112092002271.

Mellor G, Yamada T. 1982. Development of a turbulence closure model for geophysical fluid problems. *Reviews of Geophysics* **20**(4): 851–875.

Meyers J, Meneveau C. 2010. Large Eddy Simulations of large wind-turbine arrays in the atmospheric boundary layer. *AIAA Paper* **827**(January).

Meyers J, Meneveau C. 2013. Flow visualization using momentum and energy transport tubes and applications to turbulent flow in wind farms. *J. Fluid Mech.* **715**: 335–358, doi:10.1017/jfm.2012.523.

Miller LM, Brunsell Na, Mechem DB, Gans F, Monaghan AJ, Vautard R, Keith DW, Kleidon A. 2015. Two methods for estimating limits to large-scale wind power generation. *Proceedings of the National Academy of Sciences* **112**(36): 201408 251, doi:10.1073/pnas.1408251112.

Mirocha JD, Kosovic B, Aitken ML, Lundquist JK. 2014. Implementation of a generalized actuator disk wind turbine model into the weather research and forecasting model for large-eddy simulation applications. *Journal of Renewable and Sustainable Energy* **6**(1): 013104, doi:http://dx.doi.org/10.1063/1.4861061.

Moeng CH. 1984. A large-eddy-simulation model for the study of planetary boundary-layer turbulence. *J. Atmos. Sci.* **41**(13): 2052–2062, doi:10.1175/1520-0469(1984)041⟨2052:ALESMF⟩2.0.CO;2.

Muñoz Esparza D, Cañadillas B, Neumann T, van Beeck J. 2012. Turbulent fluxes, stability and shear in the offshore environment: Mesoscale modelling and field observations at FINO1. *Journal of Renewable and Sustainable Energy* **4**(6): 063 136, doi:10.1063/1.4769201.

Pope SB. 2000. *Turbulent Flows*. Cambridge University Press New York, ISBN 978-0-521-59886-6.

Porté-Agel F, Lu H, Wu YT. 2014. Interaction between Large Wind Farms and the Atmospheric Boundary Layer. *Procedia IUTAM* **10**(0): 307–318, doi:10.1016/j.piutam.2014.01.026.

Porté-Agel F, Wu YT, Lu H, Conzemius R. 2011. Large-eddy simulation of atmospheric boundary layer flow through wind turbines and wind farms. *Journal of Wind Engineering and Industrial Aerodynamics* **99**(4): 154–168, doi:10.1016/j.jweia.2011.01.011.

Rockel B, Will A, Hense A. 2008. The Regional Climate Model COSMO-CLM (CCLM). *Meteorologische Zeitschrift* **17**(4): 347–348, doi:10.1127/0941-2948/2008/0309.

Roy BS, Traiteur JJ. 2010. Impacts of wind farms on surface air temperatures. *Proceedings of the National Academy of Sciences of the United States of America* **107**(42): 17 899–904, doi:10.1073/pnas.1000493107.

Roy S. 2011. Simulating impacts of wind farms on local hydrometeorology. *Journal of Wind Engineering and Industrial Aerodynamics* **99**(4): 491–498, doi:10.1016/j.jweia.2010.12.013.

Roy S, Pacala SW, Walko RL. 2004. Can large wind farms affect local meteorology? *Journal of Geophysical Research* **109**(D19): D19 101, doi:10.1029/2004JD004763.

Schlemmer L, Hohenegger C, Schmidli J, Bretherton C, Schär C. 2011. An Idealized Cloud-Resolving Framework for the Study of Midlatitude Diurnal Convection over Land. *Journal of the Atmospheric Sciences* **68**(5): 1041–1057, doi:10.1175/2010JAS3640.1.

Schlemmer L, Hohenegger C, Schmidli J, Schär C. 2012. Diurnal equilibrium convection and land surface-atmosphere interactions in an idealized cloud-resolving model. *Quarterly Journal of the Royal Meteorological Society* **138**(667): 1526–1539, doi:10.1002/qj.1892.

Smagorinsky J. 1963. General circulation experiments with the primitive equations. *Mon. Weather Rev.* **91**(3): 99–164, doi:10.1175/1520-0493(1963)091⟨0099:GCEWTP⟩2.3.CO;2.

Stevens RJ, Graham J, Meneveau C. 2014. A concurrent precursor inflow method for large eddy simulations and applications to finite length wind farms. *Renewable Energy* **68**: 46 – 50, doi:http://dx.doi.org/10.1016/j.renene.2014.01.024.

Stull, R B. 1988. *An Introduction to Boundary Layer Meteorologyle*. Kluwer Academic Publishers, ISBN 90-277-2769-4.

Van Weverberg K, Goudenhoofdt E, Blahak U, Brisson E, Demuzere M, Marbaix P, van Ypersele JP. 2014. Comparison of one-moment and two-moment bulk microphysics for high-resolution climate simulations of intense precipitation. *Atmospheric Research* **147-148**: 145–161, doi:10.1016/j.atmosres.2014.05.012.

Vautard R, Thais F, Tobin I, Bréon FM, de Lavergne JGD, Colette A, Yiou P, Ruti PM. 2014. Regional climate model simulations indicate limited climatic impacts by operational and planned European wind farms. *Nature Communications* **5**: 1–9, doi:10.1038/ncomms4196.

Verstappen R, Veldman A. 2003. Symmetry-preserving discretization of turbulent flow. *J. Comput. Phys.* **187**(1): 343 – 368, doi:http://dx.doi.org/10.1016/S0021-9991(03)00126-8.

Volker. 2014. Wake Effects of Large Offshore Wind Farms - a study of the Mesoscale Atmosphere. PhD thesis, Technical University of Denmark.

Volker PJH, Badger J, Hahmann AN, Ott S. 2015. The explicit wake parametrisation v1.0: a wind farm parametrisation in the mesoscale model wrf. *Geoscientific Model Development* **8**(11): 3715–3731, doi:10.5194/gmd-8-3715-2015, URL http://www.geosci-model-dev.net/8/3715/2015/.

Wang C, Prinn R. 2010. Potential climatic impacts and reliability of very large-scale wind farms. *Atmospheric Chemistry and Physics* : 2053–2061.

Wu Y, Porté-Agel F. 2012. Simulation of Turbulent Flow Inside and Above Wind Farms: Model Validation and Layout Effects. *Boundary-Layer Meteorology* **146**(2): 181–205, doi:10.1007/s10546-012-9757-y.

Wu YT, Porté-Agel F. 2015. Modeling turbine wakes and power losses within a wind farm using LES: An application to the Horns Rev offshore wind farm. *Renewable Energy* **75**: 945–955, doi:10.1016/j.renene.2014.06.019.

Zhou L, Tian Y, Baidya Roy S, Thorncroft C, Bosart LF, Hu Y. 2012. Impacts of wind farms on land surface temperature. *Nature Climate Change* **2**(7): 539–543, doi:10.1038/nclimate1505.

